EarthArXiv Preprint Cover Sheet

Preprint title

Fixed-band criteria for local constant-Q models in heterogeneous fractional seismic attenuation

Authors

Ning Hu, Shuqun Li, Chengtao Huang, and Jiayan Sun

Affiliations

Ning Hu - School of Mechanical Engineering, Hangzhou Dianzi University, Hangzhou, China

Shuqun Li - School of Mathematics and Physics, Xi'an Jiaotong-Liverpool University, Suzhou, China

Chengtao Huang - School of Mechanical Engineering, Hangzhou Dianzi University, Hangzhou, China

Jiayan Sun - School of Mathematics and Physics, Wenzhou University, Wenzhou, China

Corresponding author

Ning Hu, jluhooning@163.com

Fixed-band criteria for local constant-Q models in heterogeneous fractional seismic attenuation

Ning Hu[1,*] Shuqun Li[2] Chengtao Huang[1] Jiayan Sun[3]

[1]School of Mechanical Engineering, Hangzhou Dianzi University, Hangzhou, China

[2]School of Mathematics and Physics, Xi'an Jiaotong-Liverpool University, Suzhou, China

[3]School of Mathematics and Physics, Wenzhou University, Wenzhou, China

[*]Corresponding author: Ning Hu, jluhooning@163.com

E-mail addresses: Shuqun.Li24@student.xjtlu.edu.cn (S.L.); 25010330@hdu.edu.cn (C.H.) susieee6sun@hotmail.com (J.S.)

July 18, 2026

Abstract

Local constant-Q models are widely used to describe seismic attenuation, but their validity is unclear when attenuation and dispersion vary spatially over the wavelengths being modelled. Variable-order fractional wave models can represent such heterogeneity, yet no quantitative criterion relates spatial order variation to the departure from local constant-Q behaviour. We derive a branch-resolved fixed-band criterion for a space–time fractional attenuation model with spatially varying temporal order $\alpha(x)$ and spatial order $\beta(x)$. On the causal-passive branch the frozen medium has an exactly frequency-independent local quality factor $Q_0(x)$. In one-dimensional graded media, and in a weak-attenuation multidimensional setting built on a caustic-free real geometric-optics phase, the local deviation satisfies

$$Q(x,\omega) = Q_0(x) + R(x,\omega), \qquad \|R\| \le C(\|\nabla\alpha\| + \|\nabla\beta\|)$$

over a prescribed seismic band. The wavelength-normalized order gradient $\mathcal{I}_U$ thus serves as the controlling parameter for local constant-Q validity. The same branch relation shows that Q alone leaves a one-parameter trade-off between α and β, whereas adding phase-velocity dispersion identifies the two-order description. Regional averaging is controlled for small order oscillations but can produce $O(1)$ local-Q errors across sharp contrasts. One-dimensional experiments recover the predicted first-order scaling, and nonseparable two-dimensional tests show the same gradient-controlled behaviour in a smooth low-Q anomaly.

The criterion provides a screen for deciding where local constant-Q modelling is defensible; sharp interfaces and global caustic propagation remain outside the theory.

Key words: seismic attenuation; wave propagation; fractional wave equation; variable-order operators; WKB analysis.

1 Introduction

1.1 Background and motivation

Seismic waves lose energy as they propagate, and many crustal and exploration-scale analyses treat the quality factor Q as approximately frequency independent over the seismic band. Kjartansson's (1979) constant-Q model gives a causal power-law description of this regime and motivates fractional wave equations for attenuating media. Two related formulations are central for the present work: fractional time-derivative models (Carcione et al., 2002) and the decoupled fractional-Laplacian formulation of Zhu and Harris (2014), which separates amplitude loss from phase delay using two fractional Laplacian terms whose orders depend on the local Q.

To connect frequency-dependent attenuation with velocity dispersion, we evaluate a related space–time fractional effective model. Unlike the Zhu–Harris decoupled fractional-Laplacian equation, this model places temporal memory and effective spatial nonlocality in the two orders α and β. The admissibility condition $\alpha + \beta > 2$ and the two-order manifold below are derived for the present operator.

We use α and β as effective attenuation–dispersion parameters rather than a complete rock-physics constitutive description. The order α parameterizes temporal memory and intrinsic attenuation, while β parameterizes effective spatial nonlocality and the departure of the attenuation–dispersion pair from the local $\beta = 2$ reference. Small departures of β from 2 can be interpreted as a band-limited way to represent phase dispersion associated with unresolved layering, mesoscopic fluid exchange in partially saturated rock, multiple scattering or other multiscale elastic heterogeneity (White, 1975). They are not treated as a direct microscopic scattering law. The frozen branches used below are selected by passivity, forward propagation, and Kramers–Kronig compatibility, as in causal power-law and constant-Q attenuation theories (Caputo, 1967; Kjartansson, 1979; Szabo, 1994; Holm and Näsholm, 2011).

In a homogeneous medium the orders are constant and the theory is classical. Real media are heterogeneous: $Q = Q(x)$, and therefore the fractional orders become variable, $\alpha = \alpha(x)$

and $\beta = \beta(x)$. Spatially varying orders make the operator a variable-order pseudodifferential operator, whose Fourier-side implementation is hampered by Gibbs-type artefacts. Practitioners therefore often replace variable orders by regional averages (Zhu and Harris, 2014). The variable-order near-constant-Q regime has consequently remained a heuristic, without a theorem stating when, and how accurately, a variable-order operator realizes a nearly frequency-independent Q. The criterion developed here is therefore a smooth spatial screen. It is intended for windows where the fractional orders vary slowly over the analysed wavelength, not for strong reflection interfaces or caustic-dominated propagation.

Near-constant-Q dissipative models are well developed in geophysics, from Kjartansson's power-law Q through fractional-derivative, fractional-Zener and fractional-Laplacian wave equations (Kjartansson, 1979; Carcione et al., 2002; Chen and Holm, 2004; Treeby and Cox, 2010; Zhu and Carcione, 2014; Zhu and Harris, 2014). Variable-order differentiation and fractional-Laplacian theory provide the mathematical background (Samko and Ross, 1993; Lorenzo and Hartley, 2002; Coimbra, 2003; Sun et al., 2009; Kwaśnicki, 2017; Darve et al., 2022; Jia et al., 2025). These works design, interpret or analyse attenuating wave models, but they do not quantify how spatially varying fractional orders change the local frequency dependence of Q.

We identify the frozen constant-Q branches of the two-order model and derive a fixed-band criterion for smooth order heterogeneity.

We study the following variable-order space-time fractional operator:

$$L_{\alpha,\beta}u(x,t) := {}^{C}D_t^{\alpha(x)}u(x,t) + c^2(x)(-\Delta)^{\beta(x)/2}u(x,t), \qquad (x,t) \in \Omega \times (0,T), \tag{1}$$

Here $\Omega \subset \mathbb{R}^d$ is a bounded Lipschitz domain, ${}^{C}D_t^{\alpha(x)}$ is the Caputo derivative of x-dependent order $\alpha(x) \in (1,2)$, and $(-\Delta)^{\beta(x)/2}$ is the variable-order fractional Laplacian of order $\beta(x) \in (0,2)$. In dimensional variables the coefficient multiplying the spatial term has units $L^{\beta(x)}T^{-\alpha(x)}$. The present notation uses the nondimensional coefficient $c^2(x)$ introduced below.

The operator in (1) admits a local constant-Q interpretation only in a restricted branch and smooth-heterogeneity regime. In frozen coefficients we identify the admissible branch, the exact Q_0, and the one-parameter family of orders that realizes a prescribed quality factor. In smoothly heterogeneous media we estimate $Q(x,\omega) - Q_0(x)$ over a fixed band and quantify the error made when variable orders are replaced by regional averages.

Evaluating the derived bounds over a targeted wavelength gives a screening criterion. We measure the order variation over roughly one seismic wavelength by

$$\mathcal{I}_U = \big(\|\nabla\alpha\|_{L^\infty(U)} + \|\nabla\beta\|_{L^\infty(U)}\big) \sup_{U\times[\omega_1,\omega_2]} |k(x,\omega)|^{-1}. \tag{1.1}$$

In dimensional variables the wavelength factor is

$$\sup_{U\times[f_1,f_2]} (|k_{\mathrm{phys}}(x,f)|L_0)^{-1},$$

where $L_0 = v_0/f_0$ is a convenient reference wavelength for central frequency f_0 and representative velocity v_0. Small $\mathcal{I}_U$ indicates that a frozen local constant-Q interpretation can be used as a fixed-band approximation. Large $\mathcal{I}_U$, or an order jump at the wavelength scale, flags a region where local averaging is uncontrolled.

The frozen model also shows why Q alone is not enough to identify the two effective orders. A single attenuation estimate fixes a one-parameter constant-Q curve in (α,β) space. Adding the phase-velocity dispersion slope $\gamma_d = 1-\alpha/\beta$ gives an explicit inverse for (α,β).

The corresponding estimate is closed in one dimension and in a multidimensional weak-attenuation setting with a caustic-free geometric-optics phase (Theorem 5.5). The numerical sections test the frozen relation, gradient scaling, averaging failure and the two-dimensional diagnostic workflow.

2 Notation and preliminaries

$\Omega \subset \mathbb{R}^d$ is a bounded Lipschitz domain and $T > 0$. We write $\langle\xi\rangle = (1+|\xi|^2)^{1/2}$ and denote by ω_d the volume of the unit ball in $\mathbb{R}^d$. The orders satisfy the following standing assumption.

Assumption 2.1. $\alpha \in C^1(\Omega)$ with $1 < \alpha_- \le \alpha(x) \le \alpha_+ < 2$; $\beta \in C^1(\Omega)$ with $0 < \beta_- \le \beta(x) \le \beta_+ < 2$; $c \in C^1(\Omega)$ with $0 < c_- \le c(x) \le c_+$. In addition we require the admissibility condition

$$\alpha(x)+\beta(x) > 2 \quad \text{for all } x \in \overline{\Omega}, \qquad \text{implied in particular by } \alpha_- + \beta_- > 2. \tag{2}$$

This is necessary and sufficient for the selected passive branch: it ensures $\phi_0(x) = \pi(2-\alpha(x))/(2\beta(x)) \in (0,\pi/2)$ for every x, which is the condition $\kappa_I(x) > 0$ (forward propagation with positive spatial decay). In the boundary cases, $\alpha(x)+\beta(x) \downarrow 2$ gives $\phi_0 \uparrow \pi/2$ and $Q_0 \downarrow 0$ (over-damped), whereas $\alpha \uparrow 2$ gives $\phi_0 \downarrow 0$ and $Q_0 \to \infty$ (lossless). The strict bound $\alpha_+ < 2$ keeps the model strictly dissipative; the lossless boundary $\alpha = 2$ is used only as a limiting case. All numerical experiments use parameter pairs satisfying (2).

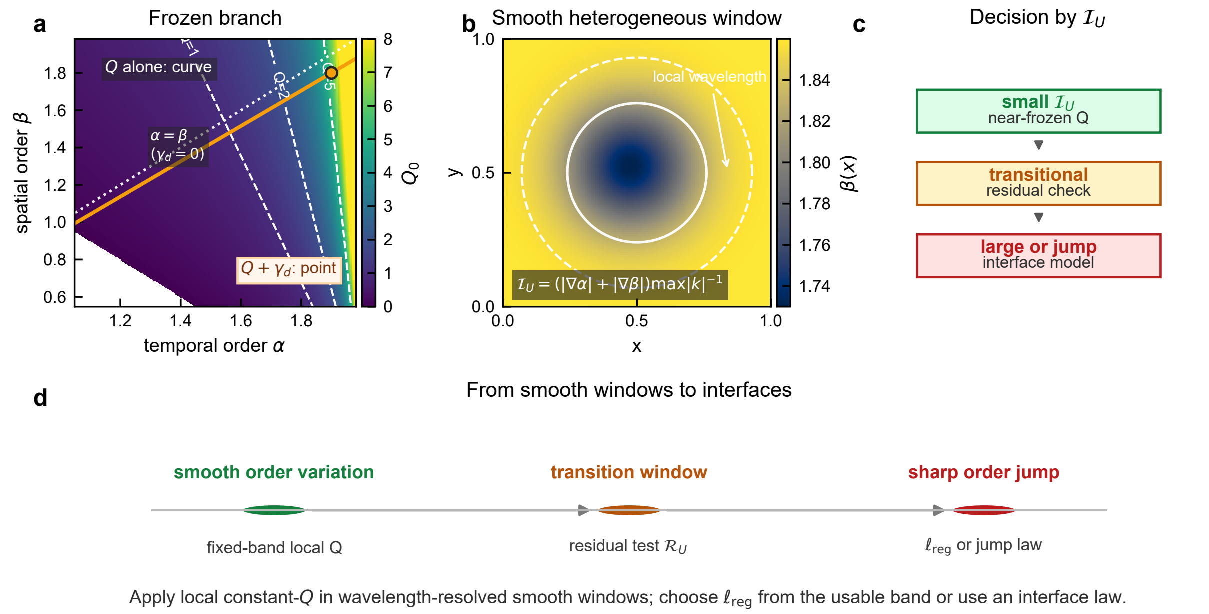

Figure 1: Schematic of the fixed-band local constant-Q criterion. (a) In the frozen model, an attenuation estimate Q_0 selects a one-parameter branch in (α, β) space, while adding the phase-velocity dispersion slope γ_d identifies the two effective orders. (b) In a smoothly heterogeneous window, order variation over the local wavelength defines the screening indicator $\mathcal{I}_U$. (c) Small $\mathcal{I}_U$ supports a local constant-Q interpretation, transitional windows require the residual check $\mathcal{R}_U$, and large gradients or jumps make regional averaging unreliable. (d) The same ordering separates wavelength-resolved smooth windows from interfaces that require residual testing, bandwidth-tied regularization length $\ell_{\rm reg}$ or an explicit transmission model.

Nondimensional reference scales. All symbols in this paper are written after fixing a reference time scale T_0 and length scale L_0. Equivalently, the frozen dispersion relation is

$$(-i\omega T_0)^{\alpha(x)} + \tilde{c}^2(x)(|\xi|L_0)^{\beta(x)} = 0, \tag{2.1}$$

and the notation below suppresses the tildes. Thus ω, ξ, and c are normalized quantities. For example, a seismic reference frequency $f_0 = 10$ Hz gives $T_0 = 1/f_0 = 0.1$ s; with a reference velocity $v_0 = 3000$ m s^{-1} one may take $L_0 = v_0 T_0 = 300$ m. A physical angular frequency $2\pi f$ is then represented by ωT_0, and a physical wavenumber by $|\xi|L_0$. Without this convention the physical dimension of $c^2(x)$ would vary with $\alpha(x)$ and $\beta(x)$, since ${}^C D_t^{\alpha(x)}$ has dimension $T^{-\alpha(x)}$ and $(-\Delta)^{\beta(x)/2}$ has dimension $L^{-\beta(x)}$. In a dimensional implementation the corresponding coefficient would have units $L^\beta T^{-\alpha}$; the present $c^2(x)$ is its nondimensional counterpart.

When β varies in space, differentiating the dimensional spatial symbol $(|\xi_{\rm phys}|L_0)^{\beta(x)}$ produces

$$\log(|\xi_{\mathrm{phys}}|L_0)\nabla\beta(x).$$

The reference length is therefore part of the model normalization, not a free unit conversion inside the estimate. For seismic use a natural default is the reference wavelength $\lambda_0 = v_0/f_0$, where f_0 is the dominant or central frequency of the analysed band and v_0 is the representative phase velocity in the window. This choice makes L_0 the length used to compare order gradients with wavelength-scale variation in $\mathcal{I}_U$. In practice the stable, transitional and uncontrolled bins in Table 1 should be recomputed, or at least reported, with the L_0, T_0 convention used for the data. If a different reference $L_0' = \rho_L L_0$ is used with the same physical data, the logarithmic coefficient changes by

$$\log(|\xi_{\mathrm{phys}}|L_0') = \log(|\xi_{\mathrm{phys}}|L_0) + \log\rho_L.$$

Thus the fixed-band constant changes at most linearly in $|\log\rho_L|$:

$$C_{I,L_0'} \le C_{I,L_0} + C_I^{(\beta)}|\log\rho_L|,$$

where $C_I^{(\beta)}$ depends on the admissible order range, passive margin, wavenumber floor and coefficient bounds on the same band. The bound is invariant only after the nondimensionalization is fixed; $\mathcal{I}_U$ and Theorem 5.5 must therefore be evaluated with the same T_0, L_0 convention as the frequency and wavenumber data.

With the 10 Hz, 3000 m s^{-1} reference above, an order change of about 0.03 across one reference wavelength gives $\mathcal{I}_U$ of order 3×10^{-2} when $|k|L_0 = O(1)$. An order change of a few tenths over the same distance moves the window into the transitional or uncontrolled range. This is the scale used below when the numerical examples compare smooth anomalies with sharp contrasts.

2.1 The variable-order Caputo derivative

For $1 < \alpha \le 2$ the Caputo derivative of a function $g \in C^2[0,T]$ is

$$^{C}D_t^{\alpha} g(t) = \frac{1}{\Gamma(2-\alpha)} \int_0^t (t-s)^{1-\alpha} g''(s)\, ds. \tag{2.2}$$

In (1) the order is the value $\alpha(x)$ frozen at the spatial point x, so for each fixed x the temporal operator is an ordinary Caputo derivative of constant order. For a steady-state time-harmonic field $e^{-i\omega t}$ one has, in the causal stationary regime (the initial Caputo transient decaying), the symbol

$$^{C}D_t^{\alpha} e^{-i\omega t} = (-i\omega)^{\alpha} e^{-i\omega t}, \qquad \omega > 0, \tag{3}$$

with the principal branch of $(-i\omega)^{\alpha}$; see Section 3. For an oscillation switched on at a finite initial time, the Caputo derivative also contains an initial-memory transient. On a fixed frequency band this contribution is asymptotically smaller than the stationary symbol and decays algebraically, of order $O(t^{-\alpha})$ for smooth harmonic data after the initial switch-on. The frequency-domain reduction below is therefore interpreted after a stationary-window time τ_{st} satisfying

$$\omega_1 \tau_{\mathrm{st}} \gg 1, \qquad \sup_{x\in U} \tau_{\mathrm{st}}^{-\alpha(x)} \ll \omega_1^{\alpha_-}.$$

Equivalently, the retained WKB terms are evaluated in windows several periods after the source turn-on, where the Caputo edge term is below the prescribed fixed-band tolerance.

Variable-order spatial operator. We use the variable-order fractional Laplacian microlocally through the symbol $c^2(x)|\xi|^{\beta(x)}$. The symbol-derivative, log-subordination and fixed-band parametrix estimates are recorded in the Supplementary Material. On a fixed seismic band, log-subordination controls logarithmic factors from $\nabla\beta$ after the reference scales T_0, L_0 have been fixed.

3 The dispersion relation and the quality factor

3.1 Frozen-coefficient dispersion relation

Fix a point x_0 and freeze the coefficients there, writing $\alpha = \alpha(x_0)$, $\beta = \beta(x_0)$, $c = c(x_0)$. We seek a time-harmonic plane-wave solution $u(x,t) = e^{i(\kappa n\cdot x - \omega t)}$ of $L_{\alpha,\beta} u = 0$, where n is a unit direction, $\omega > 0$ is the (real) angular frequency, and $\kappa \in \mathbb{C}$ is the complex wavenumber. Using (3) and $(-\Delta)^{\beta/2} e^{i\kappa n\cdot x} = \kappa^{\beta} e^{i\kappa n\cdot x}$ (principal branch along the propagation direction), substitution yields the dispersion relation

$$(-i\omega)^{\alpha} + c^2\kappa^{\beta} = 0, \qquad \text{equivalently} \qquad \kappa^{\beta} = -\frac{(-i\omega)^{\alpha}}{c^2}. \tag{5}$$

Since κ is complex (an attenuating wave), $e^{i\kappa n\cdot x}$ grows or decays exponentially and is not an L^2 eigenfunction; (5) is therefore the dispersion relation of the frozen constant-coefficient *symbol*, not an operator identity on Ω, and the multivalued κ^{β} is assigned by analytic continuation from $\operatorname{Im}\omega > 0$ to the causal passive branch.

3.2 Definition of the quality factor

Write $\kappa = \kappa_R + i\kappa_I$. For a wave $e^{i(\kappa x - \omega t)}$ travelling in the $+x$ direction, κ_R governs the phase velocity and κ_I the spatial decay. The quality factor is defined by

$$Q := \frac{\kappa_R}{2\kappa_I}, \qquad \text{equivalently} \qquad Q^{-1} = 2\tan\phi, \quad \phi := \arg\kappa. \tag{6}$$

Physical (passive, forward-propagating) waves require $\kappa_R > 0$ and $\kappa_I > 0$, i.e. $\phi \in (0, \pi/2)$, whence $Q > 0$.

4 Exact constant-Q and the two-order manifold

4.1 Branch selection

The passive branch is selected by requiring forward propagation, positive spatial decay and compatibility with the causal power-law dispersion relation. For the frozen symbol this gives $0 < \phi_0 < \pi/2$, equivalently $\alpha + \beta > 2$. The detailed branch proof is supplied in the Supplementary Material.

4.2 The exact constant-Q proposition

Proposition 4.1. *For frozen coefficients satisfying Assumption 2.1, the passive branch has complex wavenumber*

$$\kappa(\omega) = \left(\frac{\omega^\alpha}{c^2}\right)^{1/\beta} e^{i\phi}, \qquad \phi = \frac{\pi - \alpha\pi/2}{\beta} \tag{4.1}$$

independent of ω, so that the quality factor is frequency independent:

$$Q_0 = \frac{1}{2}\cot\left(\frac{\pi - \alpha\pi/2}{\beta}\right), \qquad \partial_\omega Q_0 = 0. \tag{10}$$

Remark 4.2. Proposition 4.1 expresses analytically the well-known fact that a single power law yields a constant Q (Kjartansson). Here Q_0 depends on both orders, which is the basis for the constant-Q manifold and for the deviation analysis.

4.3 Limiting cases and consistency

The limiting cases separate lossless spatial dispersion from temporal attenuation. If $\alpha = 2$, then $\phi = 0$ and $Q_0 = +\infty$. The model reduces to the classical wave operator only when $\beta = 2$; for $0 < \beta < 2$ it remains a conservative spatially fractional dispersive wave equation. The opposite edge of the admissible cone has a different physical meaning: as $\alpha + \beta \downarrow 2$, $\phi \to \pi/2$ and $Q_0 \to 0$, which is the over-damped passive boundary. For weak attenuation, taking $\alpha = 2-\delta$ with small $\delta > 0$ and $\beta = 2$ gives $\phi = \pi\delta/4$ and

$$Q_0 = \frac{1}{2}\cot(\pi\delta/4) \approx \frac{2}{\pi\delta}, \tag{4.2}$$

recovering $Q_0 \sim 2/(\pi\delta)$ as $\delta \to 0$. Hence spatial fractionality alone does not create attenuation: with $\alpha = 2$ and $\beta < 2$, the temporal symbol is real, $\kappa^\beta = \omega^2/c^2 > 0$, and $\kappa_I = 0$. Constant-Q attenuation in this model requires $\alpha \in (1, 2)$; $\beta < 2$ changes the phase-velocity dispersion, not the loss mechanism by itself.

4.4 The constant-Q manifold

Consequence 4.3. *For a prescribed target $Q_0 > 0$, the set of admissible orders is the explicit one-parameter curve*

$$\beta = \frac{\pi(2-\alpha)}{2\,\mathrm{arccot}(2Q_0)}, \qquad \alpha \in (\alpha_*(Q_0), 2), \tag{11}$$

where the left endpoint

$$\alpha_*(Q_0) := 2 - \frac{4}{\pi}\,\mathrm{arccot}(2Q_0) \in (1, 2) \tag{12}$$

is the value at which $\beta = 2$; only $\alpha > \alpha_*(Q_0)$ keeps $\beta < 2$ within the standing admissible range.

Remark 4.4. Equation (11) shows that constant-Q does not determine the pair (α, β) uniquely: there is a one-parameter family realizing any given Q_0, trading temporal against spatial fractionality. This degeneracy is relevant to inverse problems and to the choice of formulation (time-fractional vs. spatial-fractional).

4.5 Phase velocity, dispersion, and identifiability

Proposition 4.1 records the attenuation content of the frozen branch, namely the frequency-independent Q_0. The same branch also fixes the dispersion, and the two observables together resolve the order degeneracy described below.

Proposition 4.5 (Phase velocity and automatic causality)**.** *On the same passive branch, the phase velocity of the frozen plane wave is the pure power law*

$$c_\phi(\omega) = \frac{\omega}{\kappa_R(\omega)} = \frac{c^{2/\beta}}{\cos\phi}\,\omega^{\gamma_d}, \qquad \gamma_d := 1 - \frac{\alpha}{\beta}, \tag{13}$$

with group velocity $c_g = (\beta/\alpha)\,c_\phi$. *The attenuation coefficient is*

$$\kappa_I(\omega) = c^{-2/\beta} \sin\phi\, \omega^{\alpha/\beta}, \qquad \frac{\kappa_I}{\kappa_R} = \tan\phi \quad \textit{(frequency independent)}, \tag{14}$$

which is exactly the constant-Q statement $Q_0^{-1} = 2\tan\phi$. *The complex wavenumber has the closed form*

$$\kappa(\omega) = c^{-2/\beta}\, e^{i\pi/\beta}\,(-i\omega)^{\alpha/\beta}, \tag{15}$$

which is the boundary value of a function analytic in the upper half ω*-plane and polynomially bounded. Because* $\kappa \sim \omega^{\alpha/\beta}$ *grows,* κ_R *and* κ_I *are related not by an unsubtracted Hilbert transform but by a Kramers-Kronig dispersion relation with* $\lceil \alpha/\beta \rceil$ *subtractions; for the pure power law (15) this subtracted relation is equivalent to the frequency-independent phase* $\arg\kappa = \phi$, *i.e. to (14). Thus, on the frozen branch, constant Q and power-law dispersion reflect two manifestations of the same complex dispersion relation.*

Remark 4.6. The sign of γ_d is diagnostic: on the manifold (11), $\gamma_d = 0$ iff $\alpha = \beta$ (dispersionless attenuation), $\gamma_d > 0$ iff $\alpha < \beta$ (velocity increases with frequency), and $\gamma_d < 0$ iff $\alpha > \beta$. A space–time fractional model can therefore carry attenuation with either sign of velocity dispersion, whereas a purely time-fractional model ($\beta = 2$ fixed) ties the two together. This formula is used here as a fixed-band effective law. If $\gamma_d > 0$, c_ϕ and c_g grow with frequency, which is compatible only over a finite band with mechanisms such as squirt-flow-type fluid exchange or local relaxation. The power law should not be extrapolated without a high-frequency cutoff or a broader constitutive model.

The dispersion exponent supplies the missing observable. Write the two frozen observables as

$$\phi = \operatorname{arccot}(2Q_0) \;\; \text{(from attenuation)}, \qquad \gamma_d = 1 - \frac{\alpha}{\beta} \;\; \text{(from phase-velocity dispersion, (13))}. \tag{4.3}$$

Proposition 4.7 (Identifiability from attenuation and dispersion)**.** *On the admissible set* $\{1 < \alpha < 2,\ 0 < \beta < 2,\ \alpha + \beta > 2\}$ *the map* $(\alpha, \beta) \mapsto (\phi, \gamma_d)$ *is a diffeomorphism onto its image, with Jacobian*

$$\frac{\partial(\phi,\gamma_d)}{\partial(\alpha,\beta)} = -\frac{\pi}{\beta^3} \neq 0, \tag{16}$$

and inverts explicitly by

$$\beta = \frac{\pi}{\phi + \frac{\pi}{2}\,(1-\gamma_d)}, \qquad \alpha = (1-\gamma_d)\,\beta. \tag{17}$$

A single-frequency Q_0 measurement, which fixes only ϕ, leaves the manifold (11) undetermined. The pair (Q_0, γ_d), attenuation together with the dispersion slope, determines (α, β) uniquely.

Remark 4.8 (Noise propagation in the two-order inverse). Let $D = \phi + \frac{\pi}{2}(1-\gamma_d)$, so that $\beta = \pi/D$ and $\alpha = (1-\gamma_d)\beta$. Small measurement perturbations satisfy

$$\delta\beta = -\frac{\pi}{D^2}\left(\delta\phi - \frac{\pi}{2}\delta\gamma_d\right), \qquad \delta\alpha = (1-\gamma_d)\delta\beta - \beta\,\delta\gamma_d + O(|\delta\phi|^2 + |\delta\gamma_d|^2). \tag{4.4}$$

Since $Q_0 = \frac{1}{2}\cot\phi$,

$$|\delta\phi| \leq \frac{2}{1+4Q_0^2}\,|\delta Q_0| + O(|\delta Q_0|^2). \tag{4.5}$$

Thus the inverse is locally stable on compact subsets of the admissible cone with β bounded away from zero, but the recovered orders inherit phase-velocity dispersion uncertainty directly through $\delta\gamma_d$. Field use should combine the dispersion slope with phase-unwrapping quality control, bandwidth-aware regularization or prior bounds on (α, β). Failed phase unwrapping, short receiver apertures or a narrow usable band can make the dispersion slope the dominant error source. The identifiability result is a two-observable conditioning statement, not a guarantee that narrow-band or noisy phase-velocity measurements determine (α, β) robustly.

Remark 4.9. Combining attenuation and dispersion gives an explicit recovery of the effective orders. The attenuation slope gives Q_0, the phase-velocity slope gives γ_d, and (17) returns (α, β). Dispersion is the datum that breaks the degeneracy; repeated estimates of the same frequency-independent Q_0 return the same ϕ. As a check, $(\alpha, \beta) = (1.9,\ 1.8)$ gives $\gamma_d = -0.0556$, $\phi = \pi/36$ ($Q_0 = 5.715$), and (17) returns $(\alpha, \beta) = (1.900, 1.800)$; $(\alpha, \beta) = (1.7,\ 1.2)$ gives $\gamma_d = -0.4167$, $\phi = 0.3927$ ($Q_0 = 1.207$), and (17) returns $(1.700, 1.200)$–the two layers of Experiment A (Section 7.2).

Proposition 4.10 (Non-identifiability from attenuation alone)**.** *Fix $Q_0 > 0$. Any observation that determines only the frozen attenuation angle $\phi = \operatorname{arccot}(2Q_0)$, including repeated fixed-band estimates of the same frequency-independent Q_0, leaves the one-dimensional family (11) undetermined. Hence (α, β) is not identifiable from Q_0 alone; an additional dispersion observable, branch prior, or model constraint is necessary.*

5 Local WKB construction and quality-factor deviation

Spatially varying orders introduce a frequency-dependent perturbation to the frozen quality factor. We estimate that perturbation by a local phase-space WKB reduction on prescribed frequency bands where the solution admits the expansion stated below.

The small quantity is the wavelength-to-heterogeneity ratio on the fixed band. After the nondimensionalization of Section 2, let

$$\varepsilon_{\mathrm{het}} := \sup_U \left(|\nabla\alpha| + |\nabla\beta| + |\nabla \log c|\right) \sup_{\omega\in[\omega_1,\omega_2]} |k(x,\omega)|^{-1}. \tag{5.1}$$

All fixed-band constants below may depend on the passive-cone margin, the coefficient ranges, and the endpoints of the frequency band. The WKB statement is meaningful when $\varepsilon_{\mathrm{het}} \ll 1$, meaning that the order profiles vary slowly relative to the local wavelength on the prescribed seismic band.

The quality-factor estimate separates geometric heterogeneity from the variable-order source term. After the leading real transport gauge has been fixed, variations of c affect ray geometry and amplitude spreading but do not enter the branch angle defining Q_0. The Q-relevant small scale is therefore

$$\varepsilon_{\mathrm{vo}} := \sup_U \left(|\nabla\alpha| + |\nabla\beta|\right) \sup_{\omega\in[\omega_1,\omega_2]} |\kappa_0(x,\omega)|^{-1}. \tag{5.2}$$

The c-dependence remains in the constants through the wavenumber floor, ray Jacobian, and transport inverse.

The estimate requires a branch-normalized local Q and separates logarithmic order-derivative sources from ordinary variable-coefficient transport terms. It is closed in the one-dimensional graded-order setting and conditional in several dimensions, where a caustic-free complex phase and a controlled local-wavenumber remainder must be supplied.

We work in the frequency domain: a time-harmonic field $u(x,t) = v(x,\omega)e^{-i\omega t}$ satisfies

$$(-i\omega)^{\alpha(x)}v + c^2(x)(-\Delta)^{\beta(x)/2}v = 0. \tag{18}$$

5.1 WKB setting and local quality factor

We use a local WKB form $u = a(x,\omega)e^{i\omega\psi(x,\omega)}$ on an interior region U and fixed band $[\omega_1,\omega_2]$. The local complex wavenumber is $k = \omega\nabla\psi$, and $Q(x,\omega)$ is extracted from its branch-corrected real and imaginary parts. The technical admissibility assumptions are the usual fixed-band requirements: a passive-cone margin, a positive wavenumber floor, no caustic on the analysed tube and a controlled lower-order WKB remainder. The numerical diagnostics use the local plane-wave residual

$$\mathcal{R}_U(\omega) = \inf_{k_{\text{loc}}, a_{\text{loc}}} \frac{\|v - a_{\text{loc}} e^{ik_{\text{loc}}\cdot x}\|_{L^2(U)}}{\|v\|_{L^2(U)}}, \tag{5.3}$$

as a practical rejection test for windows where a branch-normalized local wavenumber is not meaningful. Here $R(x,\omega) = Q(x,\omega) - Q_0(x)$ denotes the theoretical quality-factor deviation in a window that passes the WKB assumptions, whereas $\mathcal{R}_U(\omega)$ is the numerical misfit used to reject windows before estimating Q.

5.2 Local fixed-band deviation theorem

Proposition 5.1 (Conditional local fixed-band WKB reduction)**.** *If Assumption 2.1 and the fixed-band WKB conditions described above hold on $U \times [\omega_1, \omega_2]$, the local quality factor satisfies $Q(x,\omega) = Q_0(x) + R(x,\omega)$ and*

$$\|R\|_{L^\infty(U\times[\omega_1,\omega_2])} \le C_{I,L_0}(\beta_\pm, \alpha_\pm, \omega_1, \omega_2)\left(\|\nabla\alpha\|_\infty + \|\nabla\beta\|_\infty\right), \tag{28}$$

where the constant contains the band factor $\log(\omega_2/\omega_1)/\inf_{U\times[\omega_1,\omega_2]}|k(x,\omega)|$, the WKB remainder bound and the reference-length dependence set by the nondimensional convention in Section 2. Thus the proposition is a fixed-band reduction: the constant may deteriorate as the band widens, as the lower endpoint approaches a regime where $\inf|k|$ is small, or as a different L_0 changes the logarithmic normalization. In particular, for homogeneous orders $R \equiv 0$ at the WKB order considered here, consistently with Proposition 4.1.

Remark 5.2. The estimate (28) is a conditional microlocal WKB result for smooth interior regions. It identifies the leading source of the departure from exact constant-Q behaviour in the variable-order regime. Sharp interfaces are diagnosed separately through the averaged-order error estimate of Section 6, which bounds the modelling error associated with order averaging at a jump.

5.3 Main fixed-band theorem: one dimension and weak attenuation

Proposition 5.1 is conditional in several dimensions through the existence of a caustic-free complex phase and the fixed-band local-wavenumber remainder control. The closed theorem below is therefore not a general multidimensional convergence result. It applies without further phase assumptions in one dimension, where the phase is obtained by direct integration. In higher dimensions it applies only in the weak-attenuation (high-Q) corridor, where the complex phase is a small dissipative perturbation of a caustic-free real geometric-optics phase.

Proposition 5.3 (Multidimensional complex eikonal in the weak-attenuation regime)**.** *Let $U \Subset \Omega$ with $\alpha, \beta, c \in C^\infty(U)$ satisfying the compact admissibility (8). Fix an integer $k \geq 3$, a Hölder exponent $\gamma \in (0,1)$, and a frequency band $[\omega_1, \omega_2] \Subset (0,\infty)$. Set*

$$\delta_U := \|2-\alpha\|_{C^{k,\gamma}(\overline{U})}. \tag{5.4}$$

Suppose the real eikonal

$$c^2(x)\left|\omega\nabla\psi_R(x)\right|^{\beta(x)} = \omega^{\alpha(x)}\left|\cos(\alpha(x)\pi/2)\right| \tag{34}$$

admits a real solution $\psi_R \in C^{k+1,\gamma}(\overline{U})$ whose bicharacteristic flow from a noncharacteristic entry surface Γ is a diffeomorphism onto U. More precisely, assume that the ray length is bounded by L_Γ, that $|\omega\nabla\psi_R| \geq k_0 > 0$ on $U \times [\omega_1, \omega_2]$, and that the ray Jacobian satisfies $|\det D_y x(t,y)| \geq J_0 > 0$. Then there is

$$\delta_0 = \delta_0(k, \gamma, U, \omega_1, \omega_2, \alpha_\pm, \beta_\pm, c_\pm, \|\beta\|_{C^{k,\gamma}}, \|c\|_{C^{k,\gamma}}, L_\Gamma, k_0, J_0) > 0 \tag{5.5}$$

such that whenever $\delta_U \leq \delta_0$, the complex eikonal (20) has a solution $\psi = \psi_R + \varphi \in C^{k,\gamma}(\overline{U}; \mathbb{C})$ with

$$\operatorname{Im}\psi \geq 0, \qquad \textit{no caustic in } U, \qquad \|\varphi\|_{C^{k,\gamma}(U)} + \|\operatorname{Im}\psi\|_{C^0(U)} \leq C\,\delta_U. \tag{5.6}$$

The phase, branch, no-caustic, and wavenumber-floor parts of the WKB-admissibility hypothesis of Section 5.1 then hold on $U \times [\omega_1, \omega_2]$, with constants depending only on the displayed data. Together with the lower-order remainder control recorded in the Supplementary Material, Proposition 5.1 applies there with no additional complex-phase assumption.

Remark 5.4. Proposition 5.3 retains the classical real caustic-free hypothesis used in geometric optics. In the high-Q regime this real phase determines the dissipative complex correction perturbatively. A variable-order complex parametrix through caustics and strong attenuation in $d \geq 2$ requires additional analysis.

The proof of the main theorem combines three fixed-band controls with two closed WKB corridors. The Supplementary Material fixes the causal-passive logarithm, keeps the branch away from the passive-cone boundary, makes logarithmic remainders uniform on $[\omega_1, \omega_2]$, and converts local order variation into a gradient-controlled symbol error. The phase and remainder are then closed either by the one-dimensional integral construction or by the weak-attenuation perturbation of a real caustic-free phase.

Theorem 5.5 (Main fixed-band near-constant-Q theorem)**.** *Let $[\omega_1, \omega_2] \subset (0, \infty)$ and let $U \Subset \Omega$ satisfy the compact admissibility (8). Then the branch-normalized local quality factor satisfies*

$$Q(x, \omega) = Q_0(x) + R(x, \omega), \qquad (x, \omega) \in U \times [\omega_1, \omega_2],$$

with the fixed-band estimate

$$\|R\|_{L^\infty(U\times[\omega_1,\omega_2])} \le C_{I,L_0} \left(\|\nabla\alpha\|_{L^\infty(U)} + \|\nabla\beta\|_{L^\infty(U)}\right). \tag{5.7}$$

This estimate holds in either of the following closed settings: (a) $d = 1$ with $\alpha, \beta, c \in C^1(\overline{U})$, where the complex phase is constructed directly; (b) any $d \ge 1$ in the weak-attenuation regime $\|2 - \alpha\|_{C^{k,\gamma}(\overline{U})} \le \delta_0$, provided a caustic-free real geometric-optics phase satisfies the quantitative hypotheses of Proposition 5.3. The constant C_{I,L_0} depends on the fixed band, the reference length L_0, the passive-cone margin, the relevant coefficient C^1 or $C^{k,\gamma}$ bounds, the lower order bound β_-, the wavenumber floor, and, in case (b), the real ray-Jacobian lower bound and ray-length constants of Proposition 5.3, but not on ω inside the prescribed band. In both cases $R \equiv 0$ for homogeneous orders.

5.4 Fixed-band screening rule

Theorem 5.5 yields a fixed-band criterion for local constant-Q modelling. Given order profiles $\alpha(x), \beta(x)$, a velocity scale $c(x)$, and a seismic band $[\omega_1, \omega_2]$, the user should first check the passive-cone margin $\alpha + \beta > 2 + \eta$. The next diagnostic is the wavelength-normalized heterogeneity indicator

$$\mathcal{I}_U = \left(\|\nabla\alpha\|_{L^\infty(U)} + \|\nabla\beta\|_{L^\infty(U)}\right) \sup_{U\times[\omega_1,\omega_2]} |k(x, \omega)|^{-1}. \tag{5.8}$$

Small $\mathcal{I}_U$ means that the frozen constant-Q law is expected to remain locally stable, with $Q(x, \omega)$ close to $Q_0(x)$ in the settings of Theorem 5.5. Large $\mathcal{I}_U$, or an order jump, means that regional averaging should be treated as a modelling approximation with possible $O(1)$ frozen-Q error. For field processing, choose f_0 as the centre or dominant frequency of the analysis band and take v_0 from the local phase or migration velocity model. When several bands are compared, update the reference wavelength $L_0 = v_0/f_0$ for each central frequency and recompute $k(x, \omega)$ and $\mathcal{I}_U$, rather than transporting a threshold unchanged across bands.

Table 1: Illustrative use of the fixed-band heterogeneity indicator. The regimes are asymptotic modelling bins for a chosen bandwidth, wavelength and residual criterion, not universal geological or rock-physics thresholds. The same f_0, v_0, L_0 normalization used to define the data band should be used when assigning a window to one of these bins.

Indicator regime	Mathematical reading	Modelling decision
$\mathcal{I}_U \ll 1$	Strong scale separation on the fixed band; Theorem 5.5 is expected to be a conservative local guide.	Frozen or smoothly varying local constant-Q interpretation is usually defensible after residual checks.
$\mathcal{I}_U = O(10^{-1})$	Transitional WKB regime; gradient terms may be visible and frequency-window dependence should be reported.	Use local windows and report estimator residuals; reject windows with large $\mathcal{R}_U$, especially in multi-arrival or strongly scattered zones.
$\mathcal{I}_U \gtrsim 1$ or an order jump	The small-gradient premise is weak or absent; Section 6 predicts possible $O(1)$ frozen-Q error.	Treat regional averaging as uncontrolled; use explicit transmission rules, bandwidth-tied smoothing, or a nonlocal jump formulation.

For an analysis window U and band $[\omega_1, \omega_2]$, the passive margin $\alpha(x) + \beta(x) > 2 + \eta$, the local wavenumber floor and $\mathcal{I}_U$ give the practical test. Table 1 separates windows where regional averaging is controlled from those where residual checks or interface-aware modelling are needed.

6 The averaged-order approximation

A common computational expedient replaces the variable orders $\alpha(x)$ and $\beta(x)$ by regional averages $\bar{\alpha}$ and $\bar{\beta}$ (Zhu and Harris, 2014). We quantify the resulting error at the level of the frozen local quality factor.

Consequence 6.1. *Let $\bar{Q}_0$ denote the quality factor computed from the averaged pair $(\bar{\alpha}, \bar{\beta})$ in place of $(\alpha(x), \beta(x))$. Then the relative modelling error satisfies*

$$\frac{|Q_0(x) - \bar{Q}_0|}{Q_0(x)} = O(\operatorname{osc}_\Omega \alpha + \operatorname{osc}_\Omega \beta). \tag{6.1}$$

Across a sharp Q-contrast interface, where either $\operatorname{osc} \alpha = O(1)$ or $\operatorname{osc} \beta = O(1)$, the relative error is $O(1)$ in magnitude.

Remark 6.2 (Geophysical interpretation). In geological terms, Consequence 6.1 separates smooth order variation from sharp attenuation contacts. The averaged-order approximation is accurate when both order oscillations are small. Across sharp Q contrasts it can fail by an $O(1)$ amount, exactly where strong reflectivity makes attenuation modelling sensitive. The numerical example in Section 7 shows relative errors of 59% and 95% in the two layers of a strong-contrast model. In practice, a sharp interface should either be smoothed over a bandwidth-justified length ℓ_{reg}, treated with explicit flux or transmission matching, or represented by a nonlocal jump rule. A practical choice is to tie ℓ_{reg} to the resolved band, for example $\ell_{\mathrm{reg}} \gtrsim \lambda_{\min}/2$ with $\lambda_{\min} = v_{\min}/f_2$, and then recompute $\mathcal{I}_U$ on the smoothed profile. Consequence 6.1 diagnoses the frozen-Q error caused by averaging; it does not supply the missing transmission law for a true order jump.

Consequence 6.1 bounds the frozen quality factor. Under the same compact admissibility and away from resonances, the same first-order oscillation control also governs the frequency-domain field.

Proposition 6.3 (Conditional resolvent transfer for order averaging)**.** *Fix a compact nonresonant frequency band and a common Banach pair $V \hookrightarrow H \hookrightarrow V^*$ on which both $P_{\alpha,\beta}$ and $P_{\bar{\alpha},\bar{\beta}}$ satisfy uniform resolvent bounds. Assume, in addition, the operator comparison*

$$\|P_{\alpha,\beta} - P_{\bar{\alpha},\bar{\beta}}\|_{\mathcal{L}(V,V^*)} \leq C_{\mathrm{op}}\big(\operatorname{osc}_\Omega \alpha + \operatorname{osc}_\Omega \beta\big). \tag{44}$$

If v and $\bar{v}$ solve the two problems with the same $f \in V^*$, then

$$\|v - \bar{v}\|_V \leq C\big(\operatorname{osc}_\Omega \alpha + \operatorname{osc}_\Omega \beta\big)\|f\|_{V^*}, \tag{6.2}$$

where C depends on C_{op} and the two resolvent bounds.

Remark 6.4 (The operator comparison is an additional input). The temporal multiplier satisfies the required Lipschitz estimate directly on a fixed band. For the spatial symbol, however,

$$|\xi|^{\bar{\beta}} - |\xi|^{\beta(x)} = (\bar{\beta} - \beta(x))|\xi|^{\beta(x)} \log|\xi| + O((\operatorname{osc}\beta)^2), \tag{6.3}$$

and the fixed-band log-subordination estimate controls the logarithm only with an arbitrarily small positive order loss. Thus the local symbol calculation yields (44) on a slightly stronger domain (or into a slightly weaker target), but does not by itself prove (44) on an unspecified common energy space $V \to V^*$. Establishing a lossless common-domain estimate depends on the chosen Dirichlet realization. Proposition 6.3 isolates that realization-dependent input; the unconditional averaged-order statement in this paper remains Consequence 6.1 for the frozen quality factor.

7 Numerical experiments

The numerical experiments test the frozen-Q relation, gradient dependence and averaging error on the reported Kohn–Nirenberg discretizations. The variable-order operator $\mathrm{Op}(c^2|\xi|^{\beta(x)})$ is discretized by Kohn-Nirenberg quantization on a uniform grid: with grid points x_j and discrete wavenumbers k_m, the matrix entries are

$$A_{j\ell} = N^{-1} \sum_m c^2(x_j)|k_m|^{\beta(x_j)} e^{ik_m(x_j - x_\ell)}. \tag{7.1}$$

In the homogeneous case this reproduces the Fourier multiplier to machine precision on the $N = 1024$ grid used below: the relative operator norm of the difference is 6.6×10^{-14}. This is a spatial multiplier check, so no frequency band enters the norm comparison.

Unless stated otherwise, the direct Kohn–Nirenberg computations use $\alpha = 1.8$, $c = 1$, a one-dimensional computational interval $[0, 80]$ for each solved transverse mode, grid size $N = 1024$, absorbing width $d_{\mathrm{abs}} = 16$, sponge strength $\gamma_{\max} = 8$, and a Gaussian soft source placed just inside the left absorbing layer. Complex wavenumbers are extracted by least-squares fits of $\log v$ on interior windows that exclude the source and absorbing layers; mesh-refinement tests repeat the extraction for $N = 256, \ldots, 1024$. In dimensional applications, the same $L_0 = v_0/f_0$ convention used to normalize the data band should be fixed before forming $|k_{\mathrm{phys}}|L_0$, reporting $\mathcal{I}_U$, or comparing windows across different bands. Supplementary tables list the parameters used for each experiment, and the supplementary script records the fitting windows and random seed used for the identifiability Monte Carlo.

The deterministic diagnostics used to validate the fixed-band estimates are mapped in Table 2. The main figures are supplied as PDF exports, with TIFF or PNG companions where raster panels are used.

Table 2: Organization of the deterministic numerical diagnostics.

Test (Section)	Medium and dimension	Diagnostic target
Formula (7.1)	homogeneous, 1D	exact frozen Q relation, formula (10)
Experiment A (7.2)	two-layer, 1D	averaged-order $O(1)$ error
Experiment B (7.3)	graded order, 1D	linear deviation $R \propto \|\nabla\beta\|_\infty$
Experiment C (7.4)	nonseparable smooth contrast, 2D	scattered-field scaling and local-Q diagnostics
smooth low-Q anomaly (7.4)	embedded anomaly, 2D	windowed Q_{num} and supplementary E_Q gradient scan
Experiment D (7.5)	synthetic noisy observables	identifiability inversion (Proposition 4.7)

7.1 Validation of the exact formula

The homogeneous baseline evaluates the frozen quality-factor formula (Proposition 4.1) in a controlled frequency-domain solve. With $\alpha = 1.8$, absorbing layers and a Gaussian incident wave, the complex wavenumber was extracted by least-squares fitting $\log v$ on a source-adjacent interior window. The recovered Q matches (10) to within 0.4–2.2% (Table 3):

Table 3: Homogeneous one-dimensional validation of the frozen quality-factor formula. The values are deterministic windowed extractions; the main uncertainty comes from absorbing-layer contamination, finite fitting windows and multiplier discretization.

β	1.2	1.5	1.8
Q_{num}	1.907	2.383	2.847
Q_0 (10)	1.866	2.352	2.836
relative error	2.2%	1.3%	0.4%

These discrepancies are numerical extraction errors rather than errors in the frozen formula. The main contributions are absorbing-layer contamination, the finite fitting window for $\log v$, and discretization of the fractional multiplier. The reduction of the error as β increases in this test is therefore not interpreted as a change in the exact formula, but as a change in the conditioning of the numerical wavenumber extraction.

7.2 Experiment A: averaged-order error in a strong-contrast model

A two-layer medium with $(\alpha, \beta) = (1.9, 1.8)$ and $(1.7, 1.2)$ has $Q_0 = 5.715$ and 1.207 by (10). The averaged orders $(\bar{\alpha}, \bar{\beta}) = (1.8, 1.5)$ give $\bar{Q}_0 = 2.356$, a relative error of 59% in the first layer and 95% in the second, confirming the $O(1)$ failure of Consequence 6.1 at strong contrast.

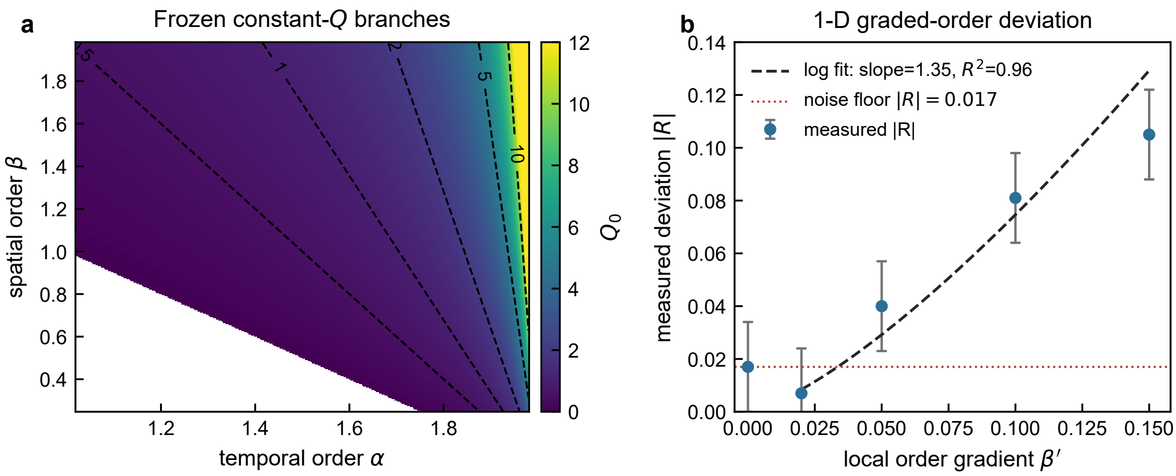

Figure 2: (a) The quality factor $Q_0(\alpha,\beta)$ of (10); black dashed curves are the constant-Q manifolds (11) for $Q_0 \in \{0.5, 1, 2, 5, 10\}$, illustrating the one-parameter trade-off between temporal and spatial fractionality. (b) The measured deviation $|R|$ of Experiment B against the local order gradient β'. Error bars show the $|R| = 0.017$ numerical floor measured at $\beta' = 0$, and the dashed fit reports the descriptive log–log slope and R^2 for the four nonzero-gradient points.

7.3 Experiment B: linear scaling of the deviation

For a graded medium with local slope β' at $\beta_0 = 1.8$ and $\omega = 2$, Table 4 reports the measured deviation $R = Q_{\text{num}} - Q_0$:

Table 4: Measured deviation in the one-dimensional graded-order experiment. The value $R = +0.017$ at $\beta' = 0$ is the numerical noise floor of the extraction procedure.

β'	0	0.02	0.05	0.10	0.15
R	+0.017	-0.007	-0.040	-0.081	-0.105

The deviation doubles from $\beta' = 0.05$ to 0.10 and vanishes (to the noise floor 0.017) as $\beta' \to 0$, supporting the linear scaling $R \propto \|\nabla\beta\|$ in the one-dimensional setting of Theorem 5.5 (Figure 2(b); panel (a) shows the corresponding $Q_0(\alpha,\beta)$ locus of (10)–(11)). The frequency dependence is nonmonotone with a maximum near $\omega \approx 2-4$, in qualitative agreement with the fixed-band envelope in (27). This one-dimensional graded-order experiment is the closed diagnostic case for the WKB scaling.

7.4 Experiment C: a nonseparable two-dimensional scattering diagnostic

The oblique-mode test above is still separable in the transverse direction. To test the actual two-dimensional Kohn–Nirenberg operator, we also implemented a small-grid direct frequency-domain scattering diagnostic in which

$$\beta(x,y)=\beta_0+\varepsilon\,\sin^2(\pi x/L)\sin^2(\pi y/L)\sin(2\pi x/L)\cos(2\pi y/L), \tag{7.2}$$

so that the order contrast is compactly supported away from the artificial boundary and is nonseparable. The discrete operator is assembled from the definition

$$\mathrm{Op}_\beta\, v(x_j)=\frac{1}{N}\sum_m e^{ix_j\cdot\xi_m}|\xi_m|^{\beta(x_j)}\widehat{v}(\xi_m), \tag{7.3}$$

with no transverse-mode reduction. We use the constant-order causal-passive branch as an incident wave $u_{\mathrm{inc}}=e^{i\kappa_0 x}$ and solve the contrast equation for the scattered correction generated by $\beta(x,y)-\beta_0$. This scattered-field formulation isolates variable-order effects by removing point-source spreading and boundary-reflection artefacts.

For $\varepsilon=0$, the constructed incident-wave baseline recovers the frozen quality factor to machine precision (median relative error 1.9×10^{-16}). For $\varepsilon\in[10^{-4},4\times10^{-4}]$, the direct linear solves have relative residuals below 6×10^{-12} and $\|w\|_2/\|u_{\mathrm{inc}}\|_2$ remains between 1.36% and 5.44%. Its log–log slope against $\|\nabla\beta\|_\infty$ is 0.999, documenting a local first-order response of this fixed finite-dimensional realization. The scattered-field norm is the reported observable because extracting a pointwise $Q_{\mathrm{num}}(x,y)$ map from a scattered field requires a separate reflection- and spreading-separated inversion step. A supplementary grid check at $N=20,24,28,32$ gives perturbative slopes between 0.9981 and 0.9992.

We also run a smooth embedded low-Q anomaly on the same nonseparable two-dimensional matrix family. The background uses $\alpha=1.8$, $\beta=1.85$, and the anomaly smoothly lowers the spatial order to $\beta_{\min}=1.7508$. The frozen branch contrast is $Q_0=2.92$ outside the anomaly and $Q_0=2.76$ at its centre. The direct solve has relative residual 2.7×10^{-13}. After applying the local plane-wave residual threshold $\mathcal{R}_U\le0.15$, with $\mathcal{R}_U(\omega)$ in (5.3), the windowed complex-wavenumber extraction gives seven accepted $Q_{\mathrm{num}}(x,y)$ samples. The median relative error is 2.63%, and the 90th-percentile relative error is 12.5%, against the frozen $Q_0(x,y)$ field (Figure 4). The larger accepted-window errors occur on the anomaly flank, where $|\nabla\beta|$ and the sensitivity to window placement are largest; the percentile tail is therefore consistent with the gradient-controlled character of $\mathcal{I}_U$. In stronger attenuation or caustic-prone regions, this residual remains a useful engineering rejection test even when the multidimensional parametrix

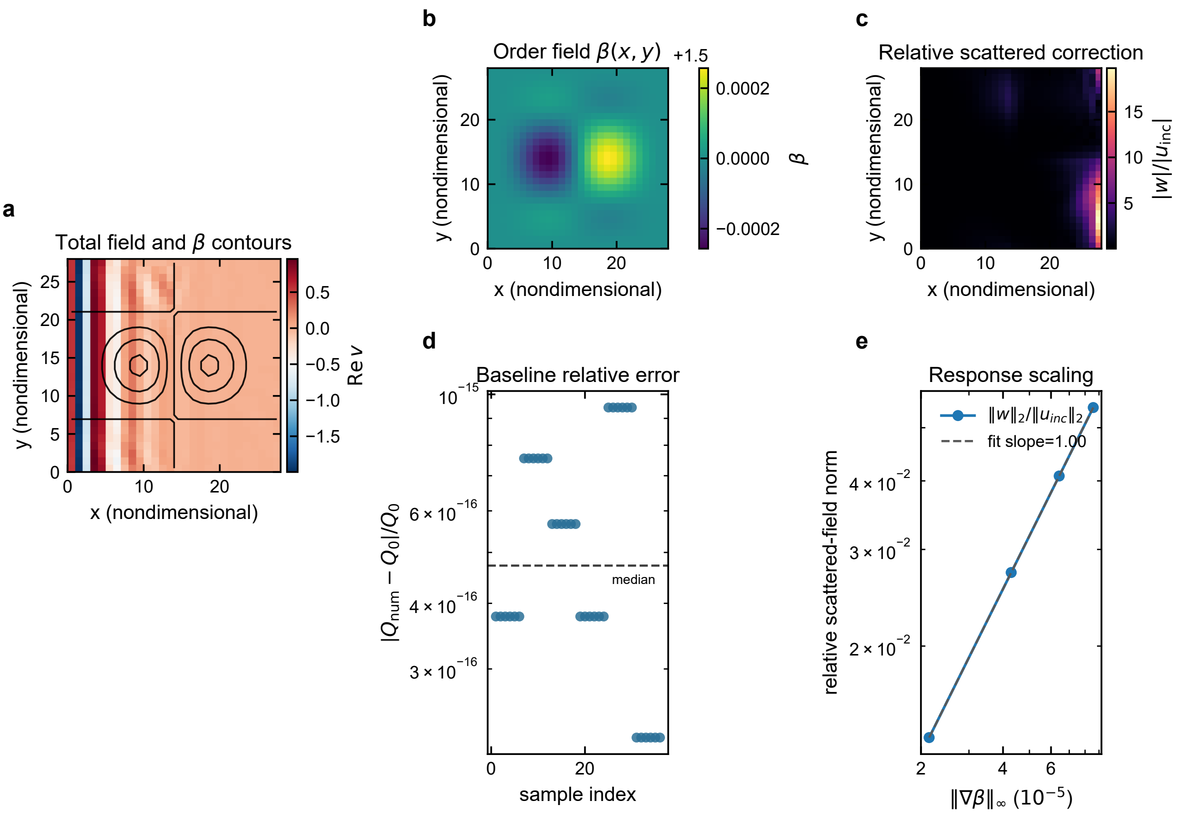

Figure 3: Nonseparable two-dimensional variable-order scattering diagnostic. (a) Real part of the total field for a compact two-dimensional order contrast. Black contours show $\beta(x, y)$. (b) The nonseparable order field. (c) Relative scattered correction $|w|/|u_{\text{inc}}|$. (d) Constructed constant-order baseline: windowed complex-wavenumber extraction recovers Q_0 to machine precision when $\varepsilon = 0$; this panel checks the extraction routine. (e) Perturbative scan: for $\varepsilon \leq 4 \times 10^{-4}$ the scattered correction stays below 5.44% and has fitted slope 0.999 against $\|\nabla\beta\|_\infty$. The panel reports the finite-dimensional response of the assembled two-dimensional operator.

assumptions are not closed. It flags windows whose fitted local plane wave is incompatible with the branch-normalized model on the chosen band. The example provides a two-dimensional smooth low-Q perturbation and a local-Q extraction workflow in the WKB regime.

The same smooth-anomaly calculation was repeated over four anomaly amplitudes, using the common local windows that pass the residual criterion at every amplitude. The median observable error

$$E_Q = \text{median}\,\frac{|Q_{\text{num}} - Q_0|}{Q_0}$$

increases from 3.28% to 6.55% as $\|\nabla\beta\|_\infty$ increases from 0.0082 to 0.0164, with a fitted log–log slope $p = 0.996$. This four-amplitude common-window scan evaluates the empirical grid

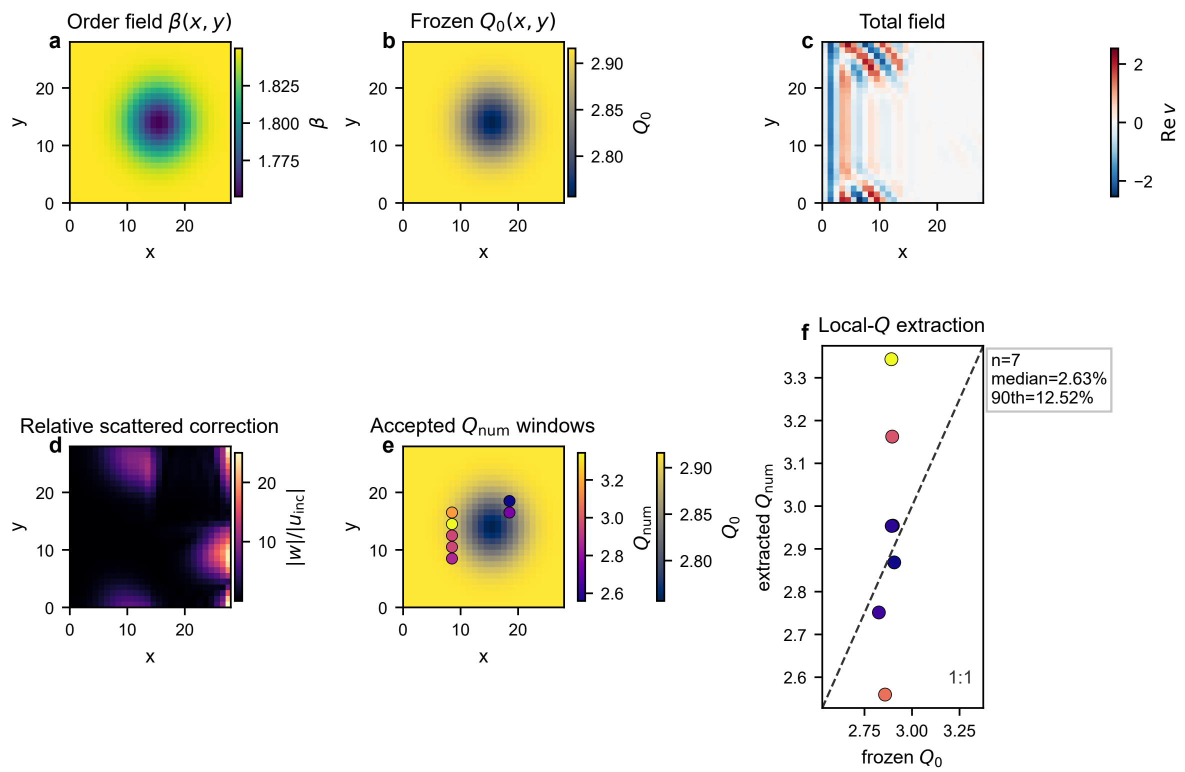

Figure 4: Smooth two-dimensional low-Q anomaly diagnostic. (a) Smooth nonseparable order anomaly; here $\alpha = 1.8$ is fixed and β varies from 1.85 in the background to 1.7508 at the anomaly centre. (b) Frozen branch quality-factor field $Q_0(x, y)$ from (10). (c) Total frequency-domain field. (d) Relative scattered correction. (e) The seven $Q_{\rm num}$ samples accepted by the $\mathcal{R}_U \leq 0.15$ local plane-wave residual criterion. (f) Extracted $Q_{\rm num}$ against frozen Q_0, with a dashed 1:1 reference line. The accepted samples have median relative error 2.63% and 90th-percentile relative error 12.5%; the largest deviations occur on the anomaly flank.

sensitivity of the extracted local Q values. The perturbation range is deliberately small; for stronger contrasts the local plane-wave residual $\mathcal{R}_U(\omega)$ should be used as a rejection diagnostic before interpreting $Q_{\rm num} - Q_0$.

The nonseparable solves test matrix assembly, algebraic residual size and the order-gradient response of $Q_{\rm num}$ for this Kohn–Nirenberg operator. The multidimensional theorem remains tied to the caustic-free weak-attenuation assumptions of Theorem 5.5; outside that corridor, the residual $\mathcal{R}_U(\omega)$ is a rejection diagnostic rather than a proof of validity.

7.5 Experiment D: identifiability inversion

We test the identifiability result of Section 4.5 numerically. From a true pair (α, β) we compute the attenuation angle and the velocity-dispersion exponent $\gamma_d = 1 - \alpha/\beta$, add independent Gaussian relative noise, and recover (α, β) from the closed inverse of Proposition 4.7. Averaging over four representative order pairs and 2000 trials each, the RMS recovery error scales approximately linearly with the input noise. The Supplementary Material reports the plot and source data. Attenuation and dispersion together therefore break the two-order degeneracy (11) in the controlled diagnostic setting. Field estimates have finite bandwidth, and phase-velocity dispersion may be substantially noisier than the perturbative levels used here. Practical use of the inverse map should include spatial smoothness, admissible order bounds and uncertainty propagation before Q compensation or imaging.

For future Q-compensated imaging, the criterion identifies smooth regions in which a local constant-Q approximation is supported and regions where interface-aware or nonlocal modelling is required.

8 Discussion and outlook

For attenuation modelling and Q-compensated imaging, the criterion is most useful as a spatial screen. In migrated images, tomography models and compensation workflows, $\mathcal{I}_U$ can be evaluated over the analysis window and frequency band before assigning a local constant-Q law. Small values support a frozen local interpretation. Large values indicate that the grid, smoothing scale or attenuation parametrization should be reconsidered. This distinction matters near salt flanks, fractured corridors and thinly layered zones, where attenuation contrasts often occur on the scale of a wavelength.

At interfaces, the smooth-window argument breaks down. A jump in α or β destroys the differentiability used in the symbol expansion, and the fractional spatial operator couples points across the contact. Regional averaging can therefore produce $O(1)$ local-Q errors, as the two-layer experiment shows. Practical algorithms should either smooth the contrast over a bandwidth-tied length ℓ_{reg}, impose explicit flux or transmission matching, or formulate a nonlocal jump condition. These interface treatments are modelling choices and should be validated against $\mathcal{I}_U$, the local residual $\mathcal{R}_U(\omega)$, and independent attenuation measurements.

A second limitation appears when the geometric-optics phase is no longer single valued. The multidimensional theorem assumes a caustic-free real phase in the weak-attenuation corridor.

In multi-path regions, the ray Jacobian degenerates and a single local complex wavenumber no longer represents the field. The residual $\mathcal{R}_U(\omega)$ then acts as a rejection test for the local plane-wave reduction. A large residual should not be interpreted as a noisy estimate of Q. If accepted as local attenuation, such windows can overcompensate amplitudes, shift event phases and introduce migration artefacts in Q-RTM or other compensation-based imaging. They require a nonlocal attenuation map, a coupled transmission construction or a separate multi-arrival estimator before local Q-compensation is applied.

The inverse use of the model adds a separate constraint. Attenuation alone selects a one-parameter curve in (α, β) space. The phase-velocity dispersion slope γ_d supplies the missing observable, but in field data it is band limited and sensitive to phase unwrapping, receiver aperture, scattering and the chosen velocity estimator. A field-facing two-order inversion should report uncertainty in both the spectral-ratio Q estimate and the dispersion slope, then propagate those uncertainties through the inverse map. When $\gamma_d > 0$, the recovered branch has phase velocity increasing with frequency. Broadband use should therefore keep the fit inside the measured band, or embed the effective law in a relaxation or causal-cutoff model, for example a squirt-flow-type relaxation, before extrapolating to higher frequencies.

Finally, the two-order description should be distinguished from the Zhu–Harris decoupled fractional-Laplacian formulation. The latter separates amplitude loss and phase delay by using two spatial fractional Laplacian terms controlled by Q. Here α represents temporal memory and β represents effective spatial nonlocality, including band-limited effects of unresolved layering, mesoscopic heterogeneity and scattering. In frozen coefficients the selected complex branch recovers the Kjartansson-type power-law mechanism. In smooth heterogeneous media, $\mathcal{I}_U$ measures when that local interpretation remains valid.

The criterion is uncontrolled when the passive-branch margin is lost, the band is too wide for moderate logarithmic constants, caustics violate the weak-attenuation construction, an order jump occurs on the wavelength scale, or $\mathcal{R}_U(\omega)$ is large. In these cases, local constant-Q modelling requires explicit error control rather than regional order averaging. Finite-dimensional requested-time Mittag–Leffler evaluators for prescribed self-adjoint semidiscrete operators are developed separately in the companion EarthArXiv preprint by Hu et al. (2026).

Data and code availability

No external empirical datasets were used. The code and source data for the deterministic diagnostics reported here are archived on Zenodo at https://doi.org/10.5281/zenodo.

21486530 (doi:10.5281/zenodo.21486530); no proprietary field data are required for the theorem or for reproducing the diagnostic figures. The archive contains the scripts, parameter files and machine-readable outputs for the quality-factor manifold, WKB coefficient, frequency-envelope, identifiability, nonseparable two-dimensional Kohn–Nirenberg and smooth low-Q anomaly diagnostics. It also includes the source data used to generate the main figures and supplementary gradient-scan checks. File-level reproduction commands are listed in the archived README. The optional k-Wave consistency code requires a separate k-Wave Python installation and is not used as evidence for the variable-order WKB theorem.

Funding and competing interests

No specific funding was received for this work. The authors declare no competing interests. All authors contributed to conceptualization, mathematical analysis, manuscript writing, and revision, and approved the final manuscript.

Acknowledgements

The variable-order symbol estimates used in this paper are recorded self-containedly in Lemmas 2.4-2.5 and Appendix A. Broader spectral applications of related variable-order operators are left to separate work. The authors used standard digital editing tools for grammar checks and script-format consistency. All mathematical derivations, numerical computations and interpretations were produced and verified by the authors.

References

Caffarelli, L. & Silvestre, L., 2007. *An extension problem related to the fractional Laplacian*, Communications in Partial Differential Equations, **32**(8), 1245–1260, doi:10.1080/03605300600987306.

Caputo, M., 1967. *Linear models of dissipation whose Q is almost frequency independent–II*, Geophysical Journal of the Royal Astronomical Society, **13**(5), 529–539, doi:10.1111/j.1365-246X.1967.tb02303.x.

Carcione, J. M., Cavallini, F., Mainardi, F., & Hanyga, A., 2002. *Time-domain modeling of constant-Q seismic waves using fractional derivatives*, Pure Appl. Geophys., **159**, 1719–1736, doi:10.1007/s00024-002-8705-z.

Chechkin, A. V., Gorenflo, R., & Sokolov, I. M., 2005. *Fractional diffusion in inhomogeneous media*, Journal of Physics A: Mathematical and General, **38**(42), L679–L684, doi:10.1088/0305-4470/38/42/L03.

Chen, W. & Holm, S., 2004. *Fractional Laplacian time-space models for linear and nonlinear lossy media exhibiting arbitrary frequency power-law dependency*, Journal of the Acoustical Society of America, **115**(4), 1424–1430, doi:10.1121/1.1646399.

Coimbra, C. F. M., 2003. *Mechanics with variable-order differential operators*, Annalen der Physik, **12**(11–12), 692–703, doi:10.1002/andp.200310032.

Darve, E., D'Elia, M., Garrappa, R., Giusti, A., & Rubio, N. L., 2022. *On the fractional Laplacian of variable order*, Fract. Calc. Appl. Anal., **25**, 15–28, doi:10.1007/s13540-021-00003-1.

Gorenflo, R., Kilbas, A. A., Mainardi, F., & Rogosin, S. V., 2020. *Mittag-Leffler Functions, Related Topics and Applications*, 2nd edn, Springer, Berlin, doi:10.1007/978-3-662-61550-8.

Holm, S. & Näsholm, S. P., 2011. *A causal and fractional all-frequency wave equation for lossy media*, Journal of the Acoustical Society of America, **130**(4), 2195–2202, doi:10.1121/1.3631626.

Hu, N., Li, S., Huang, C., & Hu, C., 2026. *Direct requested-time modelling of space–time fractional seismic attenuation on fixed operators*, EarthArXiv preprint, doi:10.31223/X5ZR3T.

Hörmander, L., 2007. *The Analysis of Linear Partial Differential Operators III: Pseudo-Differential Operators*, Classics in Mathematics, Springer, Berlin, doi:10.1007/978-3-540-49938-1.

Jia, J., Jiang, C., Li, Y., Liu, M., & Qiu, W., 2025. *Variable-order fractional wave equation: analysis, numerical approximation, and fast algorithm*, arXiv preprint arXiv:2511.06014, doi:10.48550/arXiv.2511.06014.

Kjartansson, E., 1979. *Constant Q-wave propagation and attenuation*, J. Geophys. Res., **84**, 4737–4748, doi:10.1029/JB084iB09p04737.

Kwaśnicki, M., 2017. *Ten equivalent definitions of the fractional Laplace operator*, Fractional Calculus and Applied Analysis, **20**(1), 7–51, doi:10.1515/fca-2017-0002.

Leopold, H.-G., 1989. *On Besov spaces of variable order of differentiation*, Zeitschrift für Analysis und ihre Anwendungen, **8**(1), 69–82, doi:10.4171/ZAA/337.

Leopold, H.-G. & Schrohe, E., 1993. *Spectral invariance for algebras of pseudodifferential operators on Besov–Triebel–Lizorkin spaces*, Manuscripta Mathematica, **78**(1), 99–110, doi:10.1007/BF02599303.

Lorenzo, C. F. & Hartley, T. T., 2002. *Variable order and distributed order fractional operators*, Nonlinear Dynamics, **29**(1–4), 57–98, doi:10.1023/A:1016586905654.

Robertsson, J. O. A., Blanch, J. O., & Symes, W. W., 1994. *Viscoelastic finite-difference modeling*, Geophysics, **59**(9), 1444–1456, doi:10.1190/1.1443701.

Samko, S. G. & Ross, B., 1993. *Integration and differentiation to a variable fractional order*, Integral Transforms and Special Functions, **1**(4), 277–300, doi:10.1080/10652469308819027.

Shubin, M. A., 2001. *Pseudodifferential Operators and Spectral Theory*, 2nd edn, Springer, Berlin, doi:10.1007/978-3-642-56579-3.

Stein, E. M., 1993. *Harmonic Analysis: Real-Variable Methods, Orthogonality, and Oscillatory Integrals*, Princeton University Press, Princeton, doi:10.1515/9781400883929.

Sun, H., Chen, W., & Chen, Y., 2009. *Variable-order fractional differential operators in anomalous diffusion modeling*, Physica A: Statistical Mechanics and its Applications, **388**(21), 4586–4592, doi:10.1016/j.physa.2009.07.024.

Szabo, T. L., 1994. *Time domain wave equations for lossy media obeying a frequency power law*, Journal of the Acoustical Society of America, **96**(1), 491–500, doi:10.1121/1.410434.

Tonn, R., 1991. *The determination of the seismic quality factor Q from VSP data: a comparison of different computational methods*, Geophys. Prospect., **39**, 1–27, doi:10.1111/j.1365-2478.1991.tb00298.x.

Treeby, B. E., & Cox, B. T., 2010. *Modeling power law absorption and dispersion for acoustic propagation using the fractional Laplacian*, J. Acoust. Soc. Am., **127**, 2741–2748, doi:10.1121/1.3377056.

White, J. E., 1975. *Computed seismic speeds and attenuation in rocks with partial gas saturation*, Geophysics, **40**(2), 224–232, doi:10.1190/1.1440520.

Zhu, T., & Carcione, J. M., 2014. *Theory and modelling of constant-Q P- and S-waves using fractional spatial derivatives*, Geophys. J. Int., **196**, 1787–1795, doi:10.1093/gji/ggt483.

Zhu, T., & Harris, J. M., 2014. *Modeling acoustic wave propagation in heterogeneous attenuating media using decoupled fractional Laplacians*, Geophysics, **79**, T105–T116, doi:10.1190/geo2013-0245.1.